



CERN-EP-2022-071  
29 March 2022

## Photoproduction of low- $p_T$ $J/\psi$ from peripheral to central Pb–Pb collisions at 5.02 TeV

ALICE Collaboration

### Abstract

An excess of  $J/\psi$  yield at very low transverse momentum ( $p_T < 0.3$  GeV/ $c$ ), originating from coherent photoproduction, is observed in peripheral and semicentral hadronic Pb–Pb collisions at a center-of-mass energy per nucleon pair of  $\sqrt{s_{NN}} = 5.02$  TeV. The measurement is performed with the ALICE detector via the dimuon decay channel at forward rapidity ( $2.5 < y < 4$ ). The nuclear modification factor at very low  $p_T$  and the coherent photoproduction cross section are measured as a function of centrality down to the 10% most central collisions. These results extend the previous study at  $\sqrt{s_{NN}} = 2.76$  TeV, confirming the clear excess over hadronic production in the  $p_T$  range  $0 - 0.3$  GeV/ $c$  and the centrality range 70–90%, and establishing an excess with a significance greater than  $5\sigma$  also in the 50–70% and 30–50% centrality ranges. The results are compared with earlier measurements at  $\sqrt{s_{NN}} = 2.76$  TeV and with different theoretical predictions aiming at describing how coherent photoproduction occurs in hadronic interactions with nuclear overlap.

arXiv:2204.10684v1 [nucl-ex] 22 Apr 2022

Diffraction photoproduction of  $J/\psi$  mesons in nucleus–nucleus collisions is sensitive to the nuclear gluon distributions at low Bjorken- $x$ , in the range  $x \sim 10^{-5}$  to  $10^{-2}$  at LHC energies, where they are still poorly constrained [1–3]. This process was extensively studied in nuclear collisions with impact parameters larger than twice the nuclear radius, known as ultra-peripheral collisions (UPCs) [4–9]. In UPCs, hadronic interactions are strongly suppressed providing a clean experimental environment to study photon-induced processes.

Photonuclear reactions are produced by the strong electromagnetic field generated by ultra-relativistic ions, which can be treated as a flux of quasi-real photons. At leading order in perturbative quantum chromodynamics (pQCD), the photon fluctuates into a quark–antiquark pair (a color dipole) [10], which probes the gluon distribution of the target via the exchange of two gluons in a singlet color state, with the dipole finally recombining into a vector meson (VM) [11, 12]. The diffractive VM photoproduction on nuclei can be either coherent or incoherent. In the coherent interaction, the photon emitted by one of the nuclei couples with the second nucleus as a whole. A VM with very low average transverse momentum ( $\langle p_T \rangle \approx 60$  MeV/ $c$ ) is produced, while the target nucleus remains intact. In incoherent photoproduction, the photon couples to a single nucleon from the second nucleus and produces a VM with larger average transverse momentum ( $\langle p_T \rangle \approx 500$  MeV/ $c$ ).

In nuclear collisions with impact parameters smaller than the sum of the radii of the colliding nuclei, production from hadronic interactions becomes the dominant contribution to the  $J/\psi$  yield. Hadroproduction of  $J/\psi$  mesons in Pb–Pb collisions is a long-standing probe of the quark–gluon plasma (QGP), a state of strongly-interacting matter characterized by quark and gluon degrees of freedom predicted by QCD to exist at high temperature and energy density. Charmonium production is affected by the QGP, and their measured yields [13–16] are explained as an interplay between suppression due to color screening [17] and recombination of charm quarks [18–20]. Finally, the charmonium yield can also be influenced by cold nuclear matter effects (CNM), which can be studied independently in p–Pb collisions [21–24].

The ALICE Collaboration reported the presence of an unexpectedly large  $J/\psi$  yield at very low  $p_T$  in peripheral Pb–Pb collisions at a center-of-mass energy per nucleon pair of  $\sqrt{s_{NN}} = 2.76$  TeV [25], which could not be explained by any combination of suppression, regeneration, and CNM effects [26]. Coherent photoproduction of  $J/\psi$  in Pb–Pb collisions with nuclear overlap was proposed as a plausible mechanism to explain this observation [25]. A similar low- $p_T$   $J/\psi$  excess was later measured by the STAR Collaboration at RHIC in Au–Au collisions at  $\sqrt{s_{NN}} = 200$  GeV and U–U collisions at  $\sqrt{s_{NN}} = 193$  GeV [27]. The STAR measurement of the  $t$ -dependence (Mandelstam variable,  $\approx p_T^2$ ) of the excess showed a strong similarity with the one measured in UPCs, also pointing to coherent photoproduction at the origin of the excess. Similar conclusions can be drawn from the recent measurement of the  $J/\psi$  yields at low  $p_T$  in Pb–Pb collisions at  $\sqrt{s_{NN}} = 5.02$  TeV by the LHCb Collaboration [28].

The concept of coherent photoproduction in a hadronic environment raises several theoretical challenges. For example, how can the coherence condition survive in the photon–nucleus interaction if the latter is broken up during the hadronic collision? Do only the (non-interacting) spectator nucleons participate in the coherent process? To what extent is the photonuclear cross section modified by target nucleons undergoing hadronic interactions and losing energy before the photoproduction occurs? How is the yield of the photoproduced  $J/\psi$  mesons, characterized by low transverse momenta, affected by interactions with the formed and fast-expanding QGP medium? The measurements mentioned above triggered novel theoretical developments [26, 29–32] based on calculations for UPCs in which the nuclear photoproduction cross section of a VM is usually computed as the product of a quasi-real photon flux with the photonuclear cross section corresponding to the  $\gamma A \rightarrow VM + A$  interaction, where  $\gamma$  is the photon and  $A$  is the nucleus. For collisions with nuclear overlap, in all considered models, an effective photon flux is introduced to take into account the geometrical constraints of a given impact-parameter range. Depending on the model, the photonuclear cross section is sometimes also modified to account for the effective size of nuclear fragments participating in the coherent process [29, 31]. Calculations from Ref. [31] highlight

the interest of measuring the cross section (and additionally its transverse momentum dependence) of the  $J/\psi$  excess towards more central collisions in order to probe possible changes of the effective size of the coherently interacting volume. Additionally, it was suggested that the measurement of the  $J/\psi$  coherent photoproduction in UPCs and in peripheral collisions in the same rapidity range at forward rapidity can be used to extract the coherent photonuclear cross section in two different Bjorken- $x$  regions, below  $10^{-4}$  and above  $10^{-2}$  at LHC energies [33].

In this Letter, the measurement of the  $J/\psi$  nuclear modification factor and the coherent photoproduction at low  $p_T$  at forward rapidity in Pb–Pb collisions at  $\sqrt{s_{NN}} = 5.02$  TeV are presented as a function of collision centrality. The larger data set compared to the one at  $\sqrt{s_{NN}} = 2.76$  TeV [25] allows for the first time the observation of a significant excess in the 50–70% and 30–50% centrality intervals. Assuming that the observed excess originates from coherent  $J/\psi$  photoproduction, the corresponding cross section is extracted as a function of the collision centrality. For centrality intervals where no significant excess could be measured, an upper limit on the cross section is reported.

The ALICE detector and its performance are described in detail in Refs. [34, 35]. In this analysis, the  $J/\psi$  production is measured at forward rapidity ( $2.5 < y < 4$ ) and down to  $p_T = 0$  in the dimuon decay channel with the forward muon spectrometer, consisting of a tracking system placed downstream of a front absorber of composite material, and a trigger system placed downstream of a muon filter made of iron. The interaction vertex is determined with the Silicon Pixel Detector (SPD), which consists of the two innermost layers of the Inner Tracking System in the central barrel. The first and second innermost layers cover the pseudorapidity ranges  $|\eta| < 2$  and  $|\eta| < 1.4$ , respectively. The V0 detector, consisting of two scintillator hodoscopes placed on both sides of the interaction point and covering the pseudorapidity range  $2.8 < \eta < 5.1$  and  $-3.7 < \eta < -1.7$ , is used for triggering, beam–gas background rejection and determination of the collision centrality, which is evaluated by fitting the signal amplitude distribution in the V0 as described in Ref. [36]. The Zero Degree Calorimeters (ZDCs) are placed on both sides of the interaction point along the beam direction at a distance of 112.5 m from it and measure the spectator protons and neutrons. The requirement of a minimum energy deposited in the two neutron calorimeters, corresponding to the expected signal from one spectator neutron, and the combined use of the V0 and ZDC timing information, suppresses the background induced by electromagnetic dissociation processes [37].

The data sample considered in this analysis, collected in 2015 and 2018, consists of events where two opposite sign muons are detected in the trigger system of the muon spectrometer, each with a  $p_T$  above the trigger threshold of 1 GeV/ $c$ , in coincidence with a minimum-bias (MB) trigger. The latter is defined by the coincidence of a signal in both arrays of the V0 detector. Events are selected in the 0–90% centrality interval, where the MB trigger is fully efficient. The data sample used for this analysis amounts to  $4 \times 10^8$  triggered Pb–Pb collisions, corresponding to an integrated luminosity of  $756 \pm 17 \mu\text{b}^{-1}$  [38], where the uncertainty is systematic (the statistical one being negligible).

$J/\psi$  candidates are formed by combining pairs of opposite-sign (OS) muon tracks reconstructed in the geometrical acceptance of the muon spectrometer ( $-4 < \eta < -2.5$ ). The muon identification is ensured by requiring that each track reconstructed in the tracking chambers match a track segment in the trigger system. The single-muon and dimuon selection criteria are the same as the ones used in previous analyses [14, 25]. The raw number of  $J/\psi$  is extracted in five centrality classes (0–10%, 10–30%, 30–50%, 50–70% and 70–90%) and two  $p_T$  ranges with the aim to study the coherent (0–0.3 GeV/ $c$ ) and the incoherent photoproduction (0.3–1 GeV/ $c$ ). The choice of the transverse momentum intervals takes into account the broadening of the reconstructed transverse momentum distribution of coherently and incoherently photoproduced  $J/\psi$ , mainly due to multiple scattering in the front absorber. The raw yield is also extracted in eight  $p_T$  intervals up to 8 GeV/ $c$  in order to estimate the hadronic contribution as explained below. The signal extraction is performed by fitting the invariant mass distribution of the OS dimuons using various combinations of functional forms for the signal and background shapes as

discussed in the following. The raw  $J/\psi$  yield and its statistical uncertainty is then determined as the average of all obtained yield values and corresponding statistical uncertainties, respectively, while the associated systematic uncertainty is taken as the standard deviation of the results. The signal is modeled through an extended Crystal Ball function or a pseudo-Gaussian with a mass-dependent width [39]. The non-Gaussian tails were fixed to the values obtained by fitting either a large sample in pp collisions at  $\sqrt{s} = 13$  TeV [40] or MC simulations where the hadroproduced  $J/\psi$  signal is embedded into real events in order to account for detector occupancy effects. In the  $p_T$  ranges 0–0.3 GeV/c and 0.3–1 GeV/c, additional sets of tails are obtained from MC simulations that use as input coherently and incoherently photoproduced  $J/\psi$  from the STARlight MC generator [41]. The background is described with either a variable-width Gaussian or the ratio of second and third order polynomials.

The nuclear modification factor in the centrality interval  $i$  and transverse momentum interval  $\Delta p_T$  is defined as

$$R_{AA}^i(\Delta p_T) = \frac{N_{J/\psi}^i(\Delta p_T)}{\text{BR}_{J/\psi \rightarrow \mu^+\mu^-} \times N_{\text{MB}}^i \times A\mathcal{E}^{i,h}(\Delta p_T) \times \langle T_{AA}^i \rangle \times \sigma_{\text{pp}}(\Delta p_T)}, \quad (1)$$

where  $N_{J/\psi}^i$  are the measured raw yields,  $A\mathcal{E}^{i,h}$  is the detector acceptance and efficiency (assuming unpolarized hadroproduction),  $\text{BR}_{J/\psi \rightarrow \mu^+\mu^-}$  is the branching ratio to muon pairs [42],  $N_{\text{MB}}^i$  is the equivalent number of MB events,  $\langle T_{AA}^i \rangle$  is the average nuclear overlap function, and  $\sigma_{\text{pp}}$  is the measured  $J/\psi$  cross section in pp collisions at the same center-of-mass energy [43].

The  $A\mathcal{E}$  values are estimated with MC simulations where the  $J/\psi$  input  $p_T$  and  $y$  distributions are adjusted to data, and separately tuned for each centrality class using an iterative procedure. The time-dependent status of the electronics channels for the tracking chambers, as well as misalignment of the detector elements, were taken into account. The efficiency of the trigger chambers was determined from data and used in the simulations. The systematic uncertainty on the  $A\mathcal{E}$  value derives from the uncertainty on the MC input  $p_T$  and  $y$  distributions and on the tracking, trigger and matching efficiency. The former was evaluated by varying the input shapes tuned on data within the statistical uncertainty and by taking into account the correlations between the  $p_T$  and  $y$  distributions. Assuming that the uncertainty related to the correlation does not depend on the collision system and energy, this uncertainty was estimated using a large pp sample [40], by comparing the  $A\mathcal{E}$  values obtained from  $p_T$  ( $y$ ) dependent input shapes extracted in narrower  $y$  ( $p_T$ ) intervals with those obtained using the corresponding shapes from the full  $y$  and  $p_T$  range. The remaining uncertainties on the  $A\mathcal{E}$  were determined following the procedure described in detail in Ref. [14].

The normalization to MB events,  $N_{\text{MB}}^i$ , is computed as the product of the number of dimuon-triggered events and the inverse of the probability of having a dimuon trigger in a MB event, for the relevant centrality class  $i$ . This probability can be obtained with two methods, as explained in Ref. [44]; the difference is taken as the systematic uncertainty.

The average nuclear overlap function and number of participants are obtained from a Glauber model fit of the V0 amplitude [45, 46]. The uncertainty on the value of the V0 signal amplitude corresponding to the most central 90% of the total hadronic Pb–Pb cross section is  $\pm 1\%$ . This uncertainty is propagated into the definition of the centrality intervals as explained in Ref. [44].

The systematic uncertainties on the  $R_{AA}$  measurement as a function of centrality are summarized in Table 1.

Figure 1 shows the  $R_{AA}$  as a function of the number of participants  $\langle N_{\text{part}} \rangle$ . The relationship between  $\langle N_{\text{part}} \rangle$ , centrality and impact parameter is provided in Table 2. The  $J/\psi$   $R_{AA}$  for  $p_T < 0.3$  GeV/c (where coherent photoproduction would be highest) and  $0.3 < p_T < 1.0$  GeV/c (where incoherent photoproduction could contribute) is compared with the  $R_{AA}$  for  $1.0 < p_T < 2.0$  GeV/c (where hadroproduction dominates). The  $J/\psi$   $R_{AA}$  in the  $p_T$  interval 0–0.3 GeV/c is significantly larger than the  $R_{AA}$  at larger

**Table 1:** Systematic uncertainties (in percent) on the  $R_{AA}$  measurement for different  $J/\psi$   $p_T$  intervals. Ranges correspond to the range of values in different centrality classes, whereas the values marked with an asterisk are independent of centrality.

$p_T$	0–0.3 GeV/c	0.3–1 GeV/c	1–2 GeV/c
Signal extraction	1.8–3.7	1.5–3.4	2.4–3.4
MC input	2.5		
Tracking eff.	0–1 + 3*		
Trigger eff.	0–1 + 2.8*	0–1 + 2.0*	0–1 + 1.5*
Matching eff.	1*		
$N_{MB}$	0.3*		
$\langle T_{AA} \rangle$	0.7–2.4		
Centrality limits	0.2–7		
pp cross section	5.8*	5.4*	5.1*

transverse momenta, except for the most central events. It reaches a value of about 10 for the most peripheral events. This large increase is similar to the one of about a factor 7 measured at a lower center-of-mass energy [25]. The measurement in the interval 0.3–1 GeV/c is compatible with the one in 1–2 GeV/c except for the most peripheral events, where it is larger by roughly 2 standard deviations ( $\sigma$ ). Further studies of the kinematic distribution of this signal could confirm the origin from incoherent photoproduction processes. Data are compared with a model [26] that includes initial  $J/\psi$  production,  $J/\psi$  regeneration, and a  $J/\psi$  photoproduction component for  $p_T < 0.3$  GeV/c. The uncertainty band of the theoretical predictions is mainly due to the variation of the shadowing factor. QGP effects on the photoproduced  $J/\psi$  are taken into account as well. The theoretical predictions well describe data in the  $p_T$  and centrality ranges considered.

The excess with respect to the expected hadronic production was quantified with the same procedure as used in Ref. [25]. For each centrality class, the hadronic  $J/\psi$  yield ( $\frac{dN_{AA}^{i,h}}{dp_T}$ ) as a function of  $p_T$  is parameterized with:

$$\frac{dN_{AA}^{i,h}}{dp_T}(p_T) = \mathcal{N} \times \frac{d\sigma_{pp}^h}{dp_T}(p_T) \times R_{AA}^{i,h}(p_T) \times A e^{i,h}(p_T). \quad (2)$$

The normalization factor  $\mathcal{N}$  is defined in such a way that the integral of the function in the  $p_T$  interval 1–8 GeV/c is equal to the measured number of  $J/\psi$  in the same interval, which is dominated by hadroproduction. The  $\frac{d\sigma_{pp}^h}{dp_T}$  is taken from a fit to the pp cross section measured by ALICE at  $\sqrt{s} = 5.02$  TeV [43] with either a power law function [47] or a Lévy–Tsallis function [48, 49].  $R_{AA}^{i,h}$  is a fit to the measured nuclear modification factor as a function of  $p_T$  for the same centrality classes as presented above. For the central to semicentral intervals (0–50%) a Woods-Saxon like function [25] is used, with the parameter  $p_T^0$  defining the 50% crossing point fixed to various values related to the  $J/\psi$  mass and average transverse momentum  $\langle p_T \rangle$ . This function was chosen since it can describe the transport model predictions for  $J/\psi$  production in heavy-ion collisions [50, 51]. For the most peripheral intervals (50–90%), where the recombination effects in the QGP are expected to be smaller, a linear and a constant function are used. The fit is performed in two  $p_T$  intervals 0.65–15 GeV/c and 1–15 GeV/c, where the hadroproduction is the main contribution, and then extrapolated to  $p_T = 0$ . For the Woods-Saxon function, the quality of the low- $p_T$  extrapolation is assessed by verifying that the functional form reproduces the measured  $R_{AA}$  in the most central events where the hadronic contribution is dominant. Finally,  $A e^{i,h}$  is a fit to the hadronic  $J/\psi$  acceptance and efficiency for the centrality class  $i$ , using a ratio of two Lévy–Tsallis functions. In order not to double-count the uncertainties on the pp cross section and on the Pb–Pb  $A\mathcal{E}$ , those were disregarded in the fit to the  $R_{AA}$ . Each combination of different parametrizations and fit ranges results in a different hadronic  $J/\psi$  distribution as a function of  $p_T$ , which is then integrated in the  $p_T$  interval

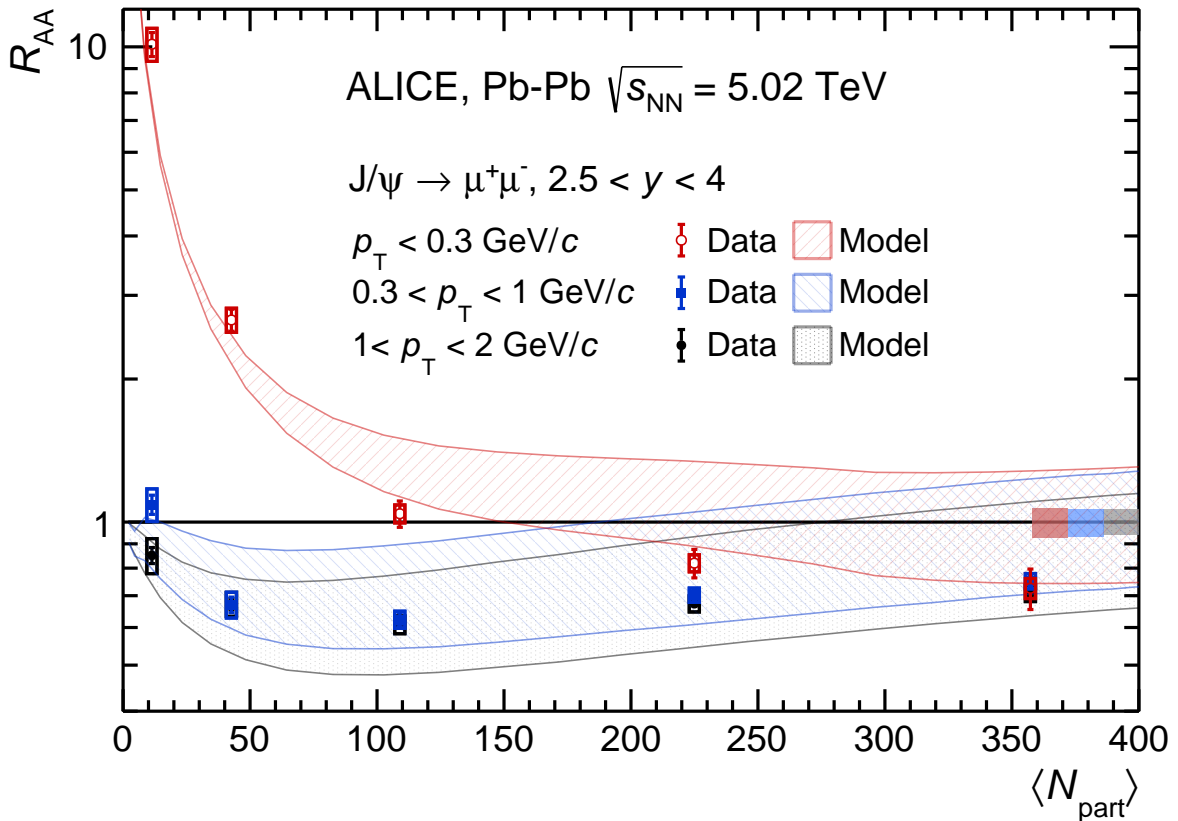


**Figure 1:**  $J/\psi$  nuclear modification factor as a function of  $\langle N_{\text{part}} \rangle$  measured in the rapidity range  $2.5 < y < 4$  for three transverse momentum intervals. The vertical bars are the statistical uncertainties and the uncorrelated systematic uncertainties are represented as boxes. The centrality-correlated systematic uncertainties are shown as filled boxes at unity. Data are compared with predictions from Ref. [26], shown as bands.

0–0.3 GeV/ $c$ . The final numbers of expected hadronic  $J/\psi$ , defined as the averages of the obtained values, are listed in Table 2 (fourth column) together with the raw measured numbers of  $J/\psi$  (third column). For the expected hadronic yields, the statistical uncertainty comes from the statistical uncertainty on  $\mathcal{N}$ , which derives from the statistical uncertainty on the  $J/\psi$  raw yield in 1–8 GeV/ $c$ . The systematic uncertainty of the expected yields is taken as the quadratic sum of the standard deviation of the results obtained using different parametrizations and fit ranges, and the average of the individual systematic uncertainties for the variations (including contributions from all factors in Eq. 2).

The estimated number of hadroproduced  $J/\psi$  is subtracted from the measured raw signal to obtain the number of  $J/\psi$  in excess (fifth column of Table 2). The measured number of  $J/\psi$  exceeds the hadronic production by  $24\sigma$  in the 70–90% centrality class,  $16\sigma$  in 50–70%,  $5.6\sigma$  in 30–50% and  $1.4\sigma$  in 10–30%. A 95% confidence interval when combining all uncertainties is provided in the centrality class 0–10% where no significant excess is observed within the current experimental uncertainties.

Assuming that the underlying process for the  $J/\psi$  excess is photoproduction, the number of coherently photoproduced  $J/\psi$  in  $0 < p_T < 0.3$  GeV/ $c$  can be extracted after correcting the excess yield for the fractions of  $J/\psi$  from incoherent photoproduction ( $f_I$ ) and from the decay of coherently photoproduced  $\psi(2S)$  ( $f_D$ ) as described in Ref. [7]. Those fractions were measured in UPC collisions at the same center-of-mass energy, although in a slightly different  $p_T$  interval,  $p_T < 0.25$  GeV/ $c$  [7]. They were therefore recomputed for  $p_T < 0.3$  GeV/ $c$ . The corresponding values and systematic uncertainties are

**Table 2:** Average number of participants, measured number of  $J/\psi$ , estimated number of hadronic  $J/\psi$ , difference between these two quantities and resulting  $J/\psi$  cross section for coherent photoproduction in the transverse momentum interval 0–0.3 GeV/ $c$  for the listed centrality classes. The first quoted uncertainty corresponds to the statistical uncertainty, the second to the centrality uncorrelated systematic uncertainty; in addition, a correlated systematic uncertainty of 6.5% applies to the cross section in all centrality classes. For the 0–10% centrality class, the quoted values corresponds to a 95% confidence level interval.

Centrality class	$\langle N_{\text{part}} \rangle$	$N_{\text{raw}}^{J/\psi}$	$N_{\text{hadro}}^{J/\psi}$	$N_{\text{excess}}^{J/\psi}$	$d\sigma_{\text{coh}}^{J/\psi}/dy$ ( $\mu\text{b}$ )
0–10%	$357.3 \pm 0.8$	$8351 \pm 762 \pm 312$	$8713 \pm 86 \pm 873$	$< 2406$ (95% CL)	$< 230$ (95% CL)
10–30%	$225.0 \pm 1.2$	$9624 \pm 571 \pm 278$	$8274 \pm 60 \pm 742$	$1350 \pm 574 \pm 792$	$145 \pm 62 \pm 85$
30–50%	$109.0 \pm 1.1$	$4280 \pm 225 \pm 105$	$2562 \pm 23 \pm 178$	$1718 \pm 226 \pm 207$	$179 \pm 24 \pm 22$
50–70%	$42.7 \mp 0.7$	$2763 \pm 98 \pm 68$	$674 \pm 8 \pm 40$	$2089 \pm 98 \pm 79$	$216 \pm 10 \pm 12$
70–90%	$11.3 \pm 0.2$	$1758 \pm 57 \pm 32$	$138 \pm 3 \pm 9$	$1620 \pm 57 \pm 33$	$167 \pm 6 \pm 12$

**Table 3:** Systematic uncertainties on the coherent  $J/\psi$  cross section (notation is the same as in Table 1).

Source	Value (%)
Branching Ratio	0.5*
$N_{\text{excess}}^{J/\psi}$	2–58.7
$f_{\text{I}}$	2.9*
$f_{\text{D}}$	1.1*
Tracking eff.	0–0.5 + 3*
Trigger eff.	0–0.5 + 3.6*
Matching eff.	1*
MC input	0.1*
$p_T$ selection	2*
Centrality limits	0.2–7
$\mathcal{L}_{\text{int}}$	2.2*

$f_{\text{I}} = 0.089 \pm 0.034$  and  $f_{\text{D}} = 0.066 \pm 0.013$ . In the following it was assumed that these fractions are the same in UPC and hadronic collisions and that they do not depend significantly on the collision centrality. The first assumption seems realistic for  $f_{\text{D}}$ , although  $f_{\text{I}}$  might vary if the coherence is incomplete in the presence of hadronic interactions.

Finally, the cross section is obtained by correcting the excess yield for the branching ratio to OS dimuons, for the  $A\mathcal{E}$  factor estimated by means of STARlight [41] simulations embedded into data for each centrality class, taking into account that the coherently photoproduced  $J/\psi$  mesons are expected to be transversely polarized, and by normalizing to the integrated luminosity and the width of the rapidity range. The systematic uncertainties are summarized in Table 3. The uncertainties on the number of excess  $J/\psi$  are discussed above. The contributions from the  $A\mathcal{E}$  are the same as in Table 1, except for the one on the STARlight MC input, which is obtained as described in Ref. [7]. An additional systematic uncertainty of 2% due to the transverse momentum resolution was estimated by comparing the  $A\mathcal{E}$  obtained with or without the  $p_T$  selection at 0.3 GeV/ $c$ . The systematic uncertainty on the luminosity mainly originates from the uncertainty of the reference V0 trigger cross section measured with van der Meer scans [38]. The uncertainties on  $f_{\text{I}}$  and  $f_{\text{D}}$  are estimated as described in Ref. [7].

The coherent  $J/\psi$  photoproduction cross section at  $\sqrt{s_{\text{NN}}} = 5.02$  TeV as a function of  $\langle N_{\text{part}} \rangle$  is shown in Figure 2. Empty boxes correspond to the uncorrelated systematic uncertainties. The correlated systematic uncertainty amounts to 6.5%, independent of centrality, and is quoted in the legend.

The result is compared with theoretical calculations that use an effective description based on UPC

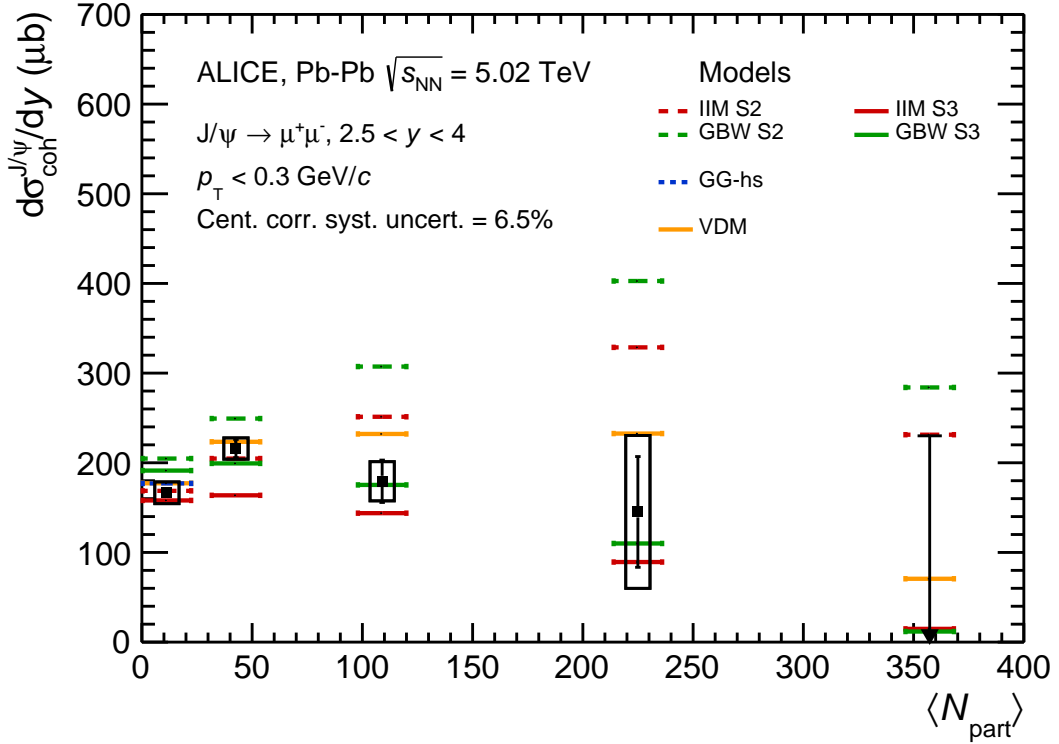


**Figure 2:**  $J/\psi$  coherent photoproduction cross section as a function of  $\langle N_{\text{part}} \rangle$  at forward rapidity in Pb–Pb collisions at  $\sqrt{s_{\text{NN}}} = 5.02$  TeV. The vertical bars are the statistical uncertainties and the uncorrelated systematic uncertainties are represented as boxes. The centrality correlated systematic uncertainties are quoted in the legend. Results are compared with theoretical calculations from Ref. [30] (GG-hs), Ref. [29] (IIM S2 and S3, and GBW S2 and S3) and from Ref. [32] with updated Glauber calculations from Ref. [52] (VDM). The figure shows the integral of the cross section measurement as well as the corresponding theoretical model values in each centrality interval. Note that the most central bin, where only an upper limit is given, is half the size of the other intervals. Therefore, to evaluate the centrality dependence of  $J/\psi$  coherent photoproduction, both data and theory have to be multiplied by a factor of two.

color dipole models. The GG-hs calculations [30] are based on energy-dependent models representing subnucleonic degrees of freedom as hot spots, and extending the calculation from protonic to nuclear targets using Glauber–Gribov formalism (GG) [30]. The photon flux is estimated in the same way as in the UPC case, but the integral is limited to the impact parameter range of the selected centrality class. The calculation from Ref. [52] is based on a vector dominance model (VDM), in which the photon fluctuates into a vector meson component that propagates through the nucleus and fragments into an on-shell vector meson. In this model, the photon flux is modified with respect to the one used in UPC calculations by considering only the photons that reach the geometrical region of the target nucleus outside of the overlap region. In the GBW calculation, the light cone color dipole formalism is used, while the IIM calculation is based on the Color Glass Condensate approach [29]. The GBW and IIM calculations provide two scenarios. In the first one (called S2 in Ref. [29]), the photon flux is modified in a similar way as for the VDM model. However, in contrast with the latter, the flux is not built by dividing over a fixed area, but over the same geometrical region as considered above. This prevents the photonuclear cross section from being progressively reduced towards more central collisions. In the second scenario (S3), an additional modification of the photonuclear cross section is introduced, in which the overlap region between the two nuclei is assumed not to contribute to coherent photoproduction resulting in significant reduction of the photoproduction cross sections towards more central collisions.



The hot-spot model prediction (GG-hs) is only available for the most peripheral centrality interval (70–90%) where the calculation is compatible with data. The other models provide predictions for all centrality intervals. The VDM model predicts a mild increase of the cross section in peripheral events, a flat evolution in semi-central events, and a decrease of the cross section in the most central events, in fair agreement with data. Notice that the figure shows the integral of the cross section in each centrality interval and the most central interval is half the size of the others. If one accounts for the interval width, the predictions for the most central interval would be twice as large, resulting in a rather mild decrease of the cross section with centrality. This model uses an optical Glauber model to describe the collision centrality, but a similar agreement with data can be obtained with a simplified relation between impact parameter and centrality [32]. The IIM and GBW models with unmodified photonuclear cross section (S2) predict a steady increase of the  $J/\psi$  coherent photoproduction cross section with centrality, once the width of the centrality intervals is properly accounted for. In data, this increasing trend is only observed for the two most peripheral intervals. In this scenario, the GBW model overestimates the data in all centrality intervals. The IIM model is in agreement with data in the first two centrality intervals, while it starts to deviate from the data by  $2.1\sigma$  in the 30–50% centrality interval. The S3 version of the GBW and IIM models [29] excluding the nuclear overlap region from the photonuclear cross section calculation predicts a decrease of the cross section from semicentral to central events (similar to the one of Ref. [52], which, however, requires only a modification of the photon flux), and is compatible with the data in the full centrality range considering the current uncertainties. It is worth noting that this centrality-dependent modification of the photonuclear cross section would result in a broadening of the  $p_T$  distribution of the  $J/\psi$  photoproduction towards more central events. A measurement of the  $J/\psi$   $p_T$  distribution at low  $p_T$  is therefore needed to clarify what is the underlying mechanism leading to the observed distribution as a function of centrality.

The models described here provided predictions also for the measurement at  $\sqrt{s_{NN}} = 2.76$  TeV [25]. The corresponding figure can be found in the Appendix A. The ratio of the measurements at  $\sqrt{s_{NN}} = 5.02$  TeV and  $\sqrt{s_{NN}} = 2.76$  TeV [25] is shown in Fig. 3. In the ratio, only the systematic uncertainty on the branching ratio cancels out. The centrality uncorrelated (correlated) systematic uncertainties in Table 3 are represented as open (filled) boxes in Fig. 3. The centrality correlated uncertainties are mainly due to the uncertainty on  $f_I$  and  $f_D$ , which were asymmetric in the estimation performed at  $\sqrt{s_{NN}} = 2.76$  TeV. The cross section increase with the center-of-mass energy does not depend significantly on the centrality. Figure 3 shows that the hot-spot model tends to underpredict the increase of the cross section with the center-of-mass energy in peripheral hadronic interactions, while the other models are in fair agreement with the measured ratio in all centrality ranges within the large uncertainties. For the IIM and GBW models no distinction is done in this case between the scenarios with or without modification of the photonuclear cross section since their energy dependence is exactly the same.

In summary, this Letter reports the measurement of  $J/\psi$  production at very low  $p_T$  as a function of centrality in hadronic Pb–Pb collisions at  $\sqrt{s_{NN}} = 5.02$  TeV at forward rapidity. The nuclear modification factor  $R_{AA}$  shows a large enhancement of the  $J/\psi$  yield for  $p_T < 0.3$  GeV/ $c$  with respect to expectations from hadronic production. This excess, which was previously seen in more peripheral collisions, is now confirmed to be present for most of the total hadronic cross section, including in collisions with a large nuclear overlap, down to at least a level of 30% in centrality. The enhancement has a significance of  $24\sigma$  in the 70–90% centrality class,  $16\sigma$  in 50–70% and  $5.6\sigma$  in the centrality class 30–50%. The reported observation extends previous measurements performed by the ALICE, LHCb and STAR Collaborations, supporting coherent photoproduction in hadronic collisions as the underlying mechanism. Based on this assumption, the corresponding cross section is extracted for the centrality classes 10–30%, 30–50%, 50–70% and 70–90% while an upper limit is given for 0–10%. The ratio of coherent photoproduction cross sections for  $\sqrt{s_{NN}} = 5.02$  TeV over  $\sqrt{s_{NN}} = 2.76$  TeV is extracted as a function of centrality and shows a flat dependence on impact parameter within uncertainties. A set of theoretical calculations successfully used to describe coherent photoproduction in UPC, and modified to account for geometrical constraints

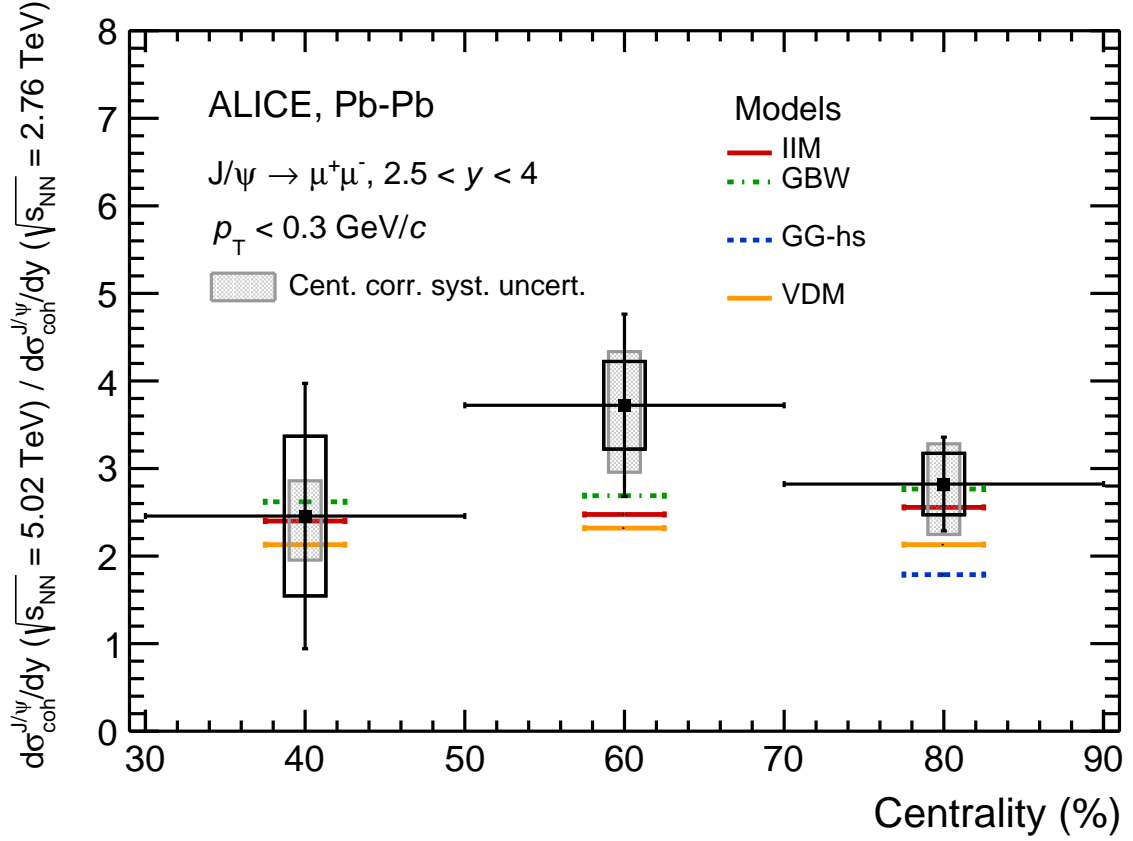


**Figure 3:**  $J/\psi$  coherent photoproduction cross section ratio for two different energies ( $\sqrt{s_{NN}} = 5.02$  TeV over  $\sqrt{s_{NN}} = 2.76$  TeV) as a function of centrality. The data at  $\sqrt{s_{NN}} = 2.76$  TeV are taken from Ref. [25]. The vertical lines are the statistical uncertainties while the open (filled) boxes are the centrality uncorrelated (correlated) systematic uncertainties. Results are compared with theoretical calculations from Ref. [30] (GG-hs), Ref. [29] (IIM and GBW) and from Ref. [32] with updated Glauber calculations from Ref. [52] (VDM).

on the photon flux in the selected centrality classes, is compared with the measurement. The cross section as a function of centrality is well described by two models, one implementing a modification of the photon flux only [52], and the other requiring an additional modification of the photonuclear cross section [29]. Additional measurements of the  $p_T$ -differential photoproduction cross section as a function of centrality and further comparison with models using different photoproduction scenarios would help to clarify the effect of the disruption of the nucleus and nucleons by hadronic interactions on the coherence condition of vector meson photoproduction.

## References

- [1] K. J. Eskola, P. Paakinen, H. Paukkunen, and C. A. Salgado, “EPPS16: Nuclear parton distributions with LHC data”, *Eur. Phys. J. C* **77** no. 3, (2017) 163, arXiv:1612.05741 [hep-ph].
- [2] V. Guzey, E. Kryshen, M. Strikman, and M. Zhalov, “Evidence for nuclear gluon shadowing from the ALICE measurements of PbPb ultraperipheral exclusive  $J/\psi$  production”, *Phys. Lett. B* **726** (2013) 290–295, arXiv:1305.1724 [hep-ph].
- [3] V. Guzey, E. Kryshen, M. Strikman, and M. Zhalov, “Nuclear suppression from coherent  $J/\psi$

- photoproduction at the Large Hadron Collider”, *Phys. Lett. B* **816** (2021) 136202, arXiv:2008.10891 [hep-ph].
- [4] ALICE Collaboration, B. Abelev *et al.*, “Coherent  $J/\psi$  photoproduction in ultra-peripheral Pb-Pb collisions at  $\sqrt{s_{NN}} = 2.76$  TeV”, *Phys. Lett. B* **718** (2013) 1273–1283, arXiv:1209.3715 [nucl-ex].
- [5] ALICE Collaboration, E. Abbas *et al.*, “Charmonium and  $e^+e^-$  pair photoproduction at mid-rapidity in ultra-peripheral Pb-Pb collisions at  $\sqrt{s_{NN}}=2.76$  TeV”, *Eur. Phys. J. C* **73** no. 11, (2013) 2617, arXiv:1305.1467 [nucl-ex].
- [6] CMS Collaboration, V. Khachatryan *et al.*, “Coherent  $J/\psi$  photoproduction in ultra-peripheral PbPb collisions at  $\sqrt{s_{NN}} = 2.76$  TeV with the CMS experiment”, *Phys. Lett. B* **772** (2017) 489–511, arXiv:1605.06966 [nucl-ex].
- [7] ALICE Collaboration, S. Acharya *et al.*, “Coherent  $J/\psi$  photoproduction at forward rapidity in ultra-peripheral Pb-Pb collisions at  $\sqrt{s_{NN}} = 5.02$  TeV”, *Phys. Lett. B* **798** (2019) 134926, arXiv:1904.06272 [nucl-ex].
- [8] ALICE Collaboration, S. Acharya *et al.*, “First measurement of the  $|t|$ -dependence of coherent  $J/\psi$  photonuclear production”, *Phys. Lett. B* **817** (2021) 136280, arXiv:2101.04623 [nucl-ex].
- [9] ALICE Collaboration, S. Acharya *et al.*, “Coherent  $J/\psi$  and  $\psi'$  photoproduction at midrapidity in ultra-peripheral Pb-Pb collisions at  $\sqrt{s_{NN}} = 5.02$  TeV”, *Eur. Phys. J. C* **81** no. 8, (2021) 712, arXiv:2101.04577 [nucl-ex].
- [10] M. G. Ryskin, “Diffractive  $J/\psi$  electroproduction in LLA QCD”, *Z. Phys. C* **57** (1993) 89–92.
- [11] S. R. Klein and H. Mäntysaari, “Imaging the nucleus with high-energy photons”, *Nature Rev. Phys.* **1** no. 11, (2019) 662–674, arXiv:1910.10858 [hep-ex].
- [12] A. J. Baltz, “The Physics of Ultraperipheral Collisions at the LHC”, *Phys. Rept.* **458** (2008) 1–171, arXiv:0706.3356 [nucl-ex].
- [13] ALICE Collaboration, B. Abelev *et al.*, “Centrality, rapidity and transverse momentum dependence of  $J/\psi$  suppression in Pb-Pb collisions at  $\sqrt{s_{NN}}=2.76$  TeV”, *Phys. Lett. B* **734** (2014) 314–327, arXiv:1311.0214 [nucl-ex].
- [14] ALICE Collaboration, J. Adam *et al.*, “Differential studies of inclusive  $J/\psi$  and  $\psi(2S)$  production at forward rapidity in Pb-Pb collisions at  $\sqrt{s_{NN}} = 2.76$  TeV”, *JHEP* **05** (2016) 179, arXiv:1506.08804 [nucl-ex].
- [15] ALICE Collaboration, S. Acharya *et al.*, “Studies of  $J/\psi$  production at forward rapidity in Pb-Pb collisions at  $\sqrt{s_{NN}} = 5.02$  TeV”, *JHEP* **02** (2020) 041, arXiv:1909.03158 [nucl-ex].
- [16] ALICE Collaboration, S. Acharya *et al.*, “Centrality and transverse momentum dependence of inclusive  $J/\psi$  production at midrapidity in Pb-Pb collisions at  $\sqrt{s_{NN}} = 5.02$  TeV”, *Phys. Lett. B* **805** (2020) 135434, arXiv:1910.14404 [nucl-ex].
- [17] T. Matsui and H. Satz, “ $J/\psi$  Suppression by Quark-Gluon Plasma Formation”, *Phys. Lett. B* **178** (1986) 416–422.
- [18] P. Braun-Munzinger and J. Stachel, “(Non)thermal aspects of charmonium production and a new look at  $J/\psi$  suppression”, *Phys. Lett. B* **490** (2000) 196–202, arXiv:nucl-th/0007059 [nucl-th].

- [19] R. L. Thews, M. Schroedter, and J. Rafelski, “Enhanced  $J/\psi$  production in deconfined quark matter”, *Phys. Rev.* **C63** (2001) 054905, arXiv:hep-ph/0007323 [hep-ph].
- [20] A. Andronic, P. Braun-Munzinger, K. Redlich, and J. Stachel, “Evidence for charmonium generation at the phase boundary in ultra-relativistic nuclear collisions”, *Phys. Lett. B* **652** (2007) 259–261, arXiv:nucl-th/0701079.
- [21] **ALICE** Collaboration, S. Acharya *et al.*, “Inclusive  $J/\psi$  production at forward and backward rapidity in p-Pb collisions at  $\sqrt{s_{NN}} = 8.16$  TeV”, *JHEP* **07** (2018) 160, arXiv:1805.04381 [nucl-ex].
- [22] **ALICE** Collaboration, S. Acharya *et al.*, “Prompt and non-prompt  $J/\psi$  production and nuclear modification at mid-rapidity in p–Pb collisions at  $\sqrt{s_{NN}} = 5.02$  TeV”, *Eur. Phys. J. C* **78** no. 6, (2018) 466, arXiv:1802.00765 [nucl-ex].
- [23] **CMS** Collaboration, A. M. Sirunyan *et al.*, “Measurement of prompt and nonprompt  $J/\psi$  production in pp and pPb collisions at  $\sqrt{s_{NN}} = 5.02$  TeV”, *Eur. Phys. J. C* **77** no. 4, (2017) 269, arXiv:1702.01462 [nucl-ex].
- [24] **LHCb** Collaboration, R. Aaij *et al.*, “Prompt and nonprompt  $J/\psi$  production and nuclear modification in pPb collisions at  $\sqrt{s_{NN}} = 8.16$  TeV”, *Phys. Lett. B* **774** (2017) 159–178, arXiv:1706.07122 [hep-ex].
- [25] **ALICE** Collaboration, J. Adam *et al.*, “Measurement of an excess in the yield of  $J/\psi$  at very low  $p_T$  in Pb-Pb collisions at  $\sqrt{s_{NN}} = 2.76$  TeV”, *Phys. Rev. Lett.* **116** no. 22, (2016) 222301, arXiv:1509.08802 [nucl-ex].
- [26] W. Shi, W. Zha, and B. Chen, “Charmonium Coherent Photoproduction and Hadroproduction with Effects of Quark Gluon Plasma”, *Phys. Lett. B* **777** (2018) 399–405, arXiv:1710.00332 [nucl-th].
- [27] **STAR** Collaboration, J. Adam *et al.*, “Observation of excess  $J/\psi$  yield at very low transverse momenta in Au+Au collisions at  $\sqrt{s_{NN}} = 200$  GeV and U+U collisions at  $\sqrt{s_{NN}} = 193$  GeV”, *Phys. Rev. Lett.* **123** no. 13, (2019) 132302, arXiv:1904.11658 [hep-ex].
- [28] **LHCb** Collaboration, R. Aaij *et al.*, “Study of  $J/\psi$  photo-production in lead-lead peripheral collisions at  $\sqrt{s_{NN}} = 5$  TeV”, arXiv:2108.02681 [hep-ex].
- [29] M. Gay Ducati and S. Martins, “Heavy meson photoproduction in peripheral AA collisions”, *Phys. Rev. D* **97** no. 11, (2018) 116013, arXiv:1804.09836 [hep-ph].
- [30] J. Cepila, J. G. Contreras, and M. Krelina, “Coherent and incoherent  $J/\psi$  photonuclear production in an energy-dependent hot-spot model”, *Phys. Rev. C* **97** no. 2, (2018) 024901, arXiv:1711.01855 [hep-ph].
- [31] W. Zha, S. R. Klein, R. Ma, L. Ruan, T. Todoroki, Z. Tang, Z. Xu, C. Yang, Q. Yang, and S. Yang, “Coherent  $J/\psi$  photoproduction in hadronic heavy-ion collisions”, *Phys. Rev. C* **97** no. 4, (2018) 044910, arXiv:1705.01460 [nucl-th].
- [32] M. Klusek-Gawenda and A. Szczurek, “Photoproduction of  $J/\psi$  mesons in peripheral and semicentral heavy ion collisions”, *Phys. Rev. C* **93** no. 4, (2016) 044912, arXiv:1509.03173 [nucl-th].
- [33] J. G. Contreras, “Gluon shadowing at small  $x$  from coherent  $J/\psi$  photoproduction data at energies available at the CERN Large Hadron Collider”, *Phys. Rev. C* **96** no. 1, (2017) 015203, arXiv:1610.03350 [nucl-ex].

- [34] **ALICE** Collaboration, K. Aamodt *et al.*, “The ALICE experiment at the CERN LHC”, *JINST* **3** (2008) S08002.
- [35] **ALICE** Collaboration, B. Abelev *et al.*, “Performance of the ALICE Experiment at the CERN LHC”, *Int. J. Mod. Phys. A* **29** (2014) 1430044, arXiv:1402.4476 [nucl-ex].
- [36] **ALICE** Collaboration, B. Abelev *et al.*, “Centrality determination of Pb-Pb collisions at  $\sqrt{s_{NN}} = 2.76$  TeV with ALICE”, *Phys. Rev. C* **88** no. 4, (2013) 044909, arXiv:1301.4361 [nucl-ex].
- [37] **ALICE** Collaboration, B. Abelev *et al.*, “Measurement of the Cross Section for Electromagnetic Dissociation with Neutron Emission in Pb-Pb Collisions at  $\sqrt{s_{NN}} = 2.76$  TeV”, *Phys. Rev. Lett.* **109** (2012) 252302, arXiv:1203.2436 [nucl-ex].
- [38] **ALICE** Collaboration, “ALICE luminosity determination for Pb–Pb collisions at  $\sqrt{s_{NN}} = 5.02$  TeV”, arXiv:2204.10148 [nucl-ex].
- [39] **ALICE** Collaboration, J. Adam *et al.*, “Quarkonium signal extraction in ALICE”, ALICE-PUBLIC-2015-006. <https://cds.cern.ch/record/2060096>.
- [40] **ALICE** Collaboration, S. Acharya *et al.*, “Energy dependence of forward-rapidity  $J/\psi$  and  $\psi(2S)$  production in pp collisions at the LHC”, *Eur. Phys. J. C* **77** no. 6, (2017) 392, arXiv:1702.00557 [hep-ex].
- [41] S. R. Klein, J. Nystrand, J. Seger, Y. Gorbunov, and J. Butterworth, “STARlight: A Monte Carlo simulation program for ultra-peripheral collisions of relativistic ions”, *Comput. Phys. Commun.* **212** (2017) 258–268, arXiv:1607.03838 [hep-ph].
- [42] **Particle Data Group** Collaboration, P. A. Zyla *et al.*, “Review of Particle Physics”, *PTEP* **2020** no. 8, (2020) 083C01.
- [43] **ALICE** Collaboration, S. Acharya *et al.*, “Inclusive quarkonium production in pp collisions at  $\sqrt{s} = 5.02$  TeV”, arXiv:2109.15240 [nucl-ex].
- [44] **ALICE** Collaboration, J. Adam *et al.*, “ $J/\psi$  suppression at forward rapidity in Pb-Pb collisions at  $\sqrt{s_{NN}} = 5.02$  TeV”, *Phys. Lett. B* **766** (2017) 212–224, arXiv:1606.08197 [nucl-ex].
- [45] **ALICE** Collaboration, J. Adam *et al.*, “Centrality dependence of the charged-particle multiplicity density at midrapidity in Pb-Pb collisions at  $\sqrt{s_{NN}} = 5.02$  TeV”, *Phys. Rev. Lett.* **116** no. 22, (2016) 222302, arXiv:1512.06104 [nucl-ex].
- [46] D. d’Enterria and C. Loizides, “Progress in the Glauber Model at Collider Energies”, *Ann. Rev. Nucl. Part. Sci.* **71** (2021) 315–344, arXiv:2011.14909 [hep-ph].
- [47] F. Bossù, Z. C. del Valle, A. de Falco, M. Gagliardi, S. Grigoryan, and G. Martinez Garcia, “Phenomenological interpolation of the inclusive  $J/\psi$  cross section to proton-proton collisions at 2.76 TeV and 5.5 TeV”, arXiv:1103.2394 [nucl-ex].
- [48] C. Tsallis, “Possible Generalization of Boltzmann-Gibbs Statistics”, *J. Statist. Phys.* **52** (1988) 479–487.
- [49] **STAR** Collaboration, B. I. Abelev *et al.*, “Strange particle production in p+p collisions at  $s^{*}(1/2) = 200$ -GeV”, *Phys. Rev. C* **75** (2007) 064901, arXiv:nucl-ex/0607033.
- [50] X. Zhao and R. Rapp, “Medium Modifications and Production of Charmonia at LHC”, *Nucl. Phys. A* **859** (2011) 114–125, arXiv:1102.2194 [hep-ph].

- [51] Y.-p. Liu, Z. Qu, N. Xu, and P.-f. Zhuang, “ $J/\psi$  Transverse Momentum Distribution in High Energy Nuclear Collisions at RHIC”, *Phys. Lett. B* **678** (2009) 72–76, [arXiv:0901.2757](#) [nucl-th].
- [52] M. Klusek-Gawenda, R. Rapp, W. Schäfer, and A. Szczurek, “Dilepton Radiation in Heavy-Ion Collisions at Small Transverse Momentum”, *Phys. Lett. B* **790** (2019) 339–344, [arXiv:1809.07049](#) [nucl-th].

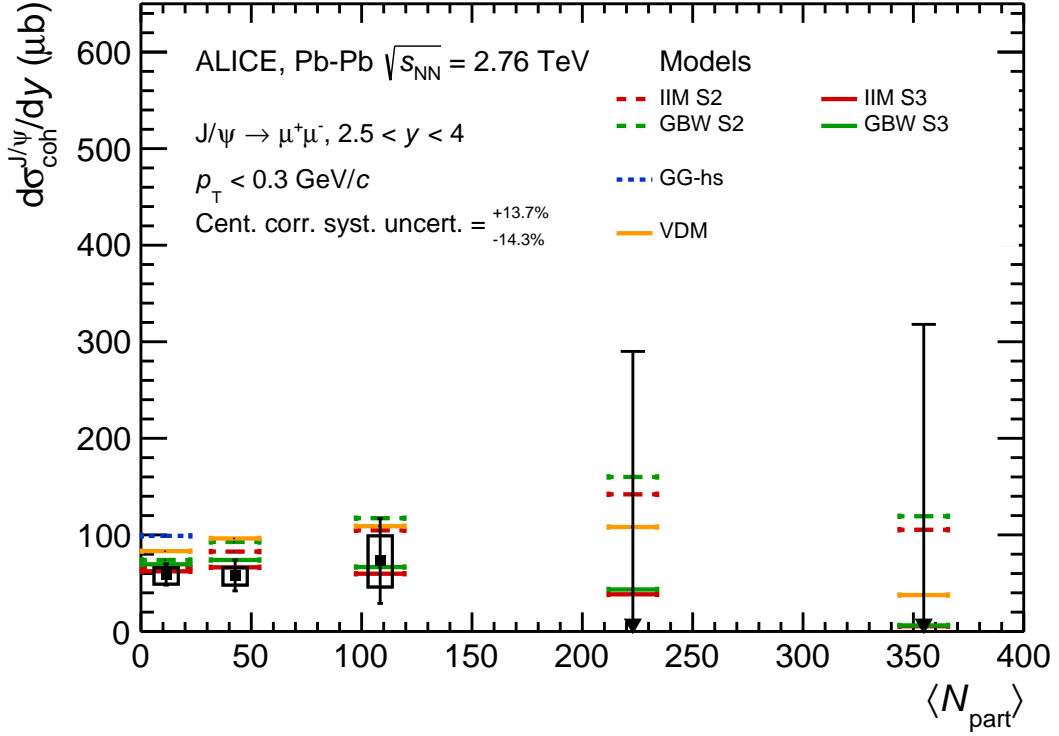


**Figure A.1:**  $J/\psi$  coherent photoproduction cross section as a function of  $\langle N_{\text{part}} \rangle$  at forward rapidity in Pb–Pb collisions at  $\sqrt{s_{\text{NN}}} = 2.76$  TeV [25]. The vertical bars are the statistical uncertainties and the uncorrelated systematic uncertainties are represented as boxes. The centrality correlated systematic uncertainties are quoted in the legend. Results are compared with theoretical calculations from Ref. [30] (GG-hs), Ref. [29] (IIM S2 and S3, and GBW S2 and S3) and from Ref. [32] with updated Glauber calculations from Ref. [52] (VDM). The figure shows the integral of the cross section measurement as well as the corresponding theoretical model values in each centrality interval. Note that the most central bin, where only an upper limit is given, is half the size of the other intervals. Therefore, to evaluate the centrality dependence of  $J/\psi$  coherent photoproduction, both data and theory have to be multiplied by a factor of two.

### A $J/\psi$ photoproduction in Pb–Pb collisions at $\sqrt{s_{\text{NN}}} = 2.76$ TeV

Figure A.1 shows the coherent photoproduction measured at  $\sqrt{s_{\text{NN}}} = 2.76$  TeV [25]. Empty boxes correspond to the uncorrelated systematic uncertainties. The centrality correlated systematic uncertainty mainly comes from the uncertainties on  $f_I$  and  $f_D$ , which are asymmetric.

The data are compared with predictions from the same set of models that were described in detail in the paper to which this appendix is associated. The hot-spot model prediction (GG-hs) [30] is only available for the most peripheral centrality interval (70–90%) and it is found to overestimate the data. The other predictions are available for all centrality intervals. The centrality dependence of the models is similar to the one shown at  $\sqrt{s_{\text{NN}}} = 5.02$  TeV. The IIM and GBW predictions [29] steadily increase with centrality in the scenario with unmodified photonuclear cross section (S2), while the use of an effective cross section where the overlap region between the two nuclei is assumed not to contribute to coherent photoproduction (S3) results in a reduction of the cross section toward more central collisions. However, both scenarios are compatible with data in the current uncertainties. Finally, the VDM calculations are in agreement with data in the most central events while they tend to overestimate data in the 50–70% and 70–90% centrality bins.